Volume XI Issue 3 Year 2026 | Page 1099-1111 | ISSN: 2527-9866
Received: 17-07-2026 | *Revised: 28-07-2026* | *Accepted: 26-08-2026*

Production and Evaluation of 360° 3D Assets Using a Mini Booth and CR-Scan Ferret

Ibrohim Yofid Fananda[1], Aji Sapta Pramulen[2], Jauari Akhmad Nur Hasim[3], Phafad Unggul Handayu[4], Irma Wulandari[5]
[1,2,3,4,5] Multimedia Broadcasting Technology Study Program, Department of Creative Multimedia Technology, Politeknik Elektronika Negeri Surabaya, Surabaya, Indonesia, 60111
e-mail: [1]ibrohim@pens.ac.id, [2]aji@pens.ac.id, [3]jauari@pens.ac.id, [4]phafad400@gmail.com, [5]irma@pens.ac.id
*Correspondence: *ibrohim@pens.ac.id*

Abstract: *This study documents and evaluates an end-to-end workflow for producing 30 textured three-dimensional (3D) assets from small-scale objects (maximum dimension 50 cm) using the active Near-Infrared scanner Creality CR-Scan Ferret inside a mini booth with diffuse lighting. Raw data were processed in Creality Scan and Blender through artifact elimination, remesh/retopology, mesh repairing, texture baking, and export. Digital dimensions were extracted from the model bounding box using Python and Open3D, then compared with reference physical measurements. The mean per-asset RMSE was 2.00 cm (SD = 1.61; median = 1.80; 95% CI = 1.40–2.60; range 0.02–6.18 cm). Under the internal thresholds of the study, 12 assets were rated Very Good, 11 Good, 5 Fair, and 2 Poor. Mean RMSE for Easy, Medium, and Hard objects was 1.32, 1.31, and 3.36 cm respectively; an exploratory Kruskal-Wallis test indicated a difference between categories ($H = 9.76$; $p = 0.0076$). Mesh Analysis was applied to six representative samples only. Two regular bottle models had Non-manifold Edges = 0 and Shells = 1, whereas the Hashmal model had 14,945 Non-manifold Edges and 7 Shells. The workflow is usable as an initial pipeline for digital visualization, but the results do not prove universal metric accuracy or watertightness because repeated scans, measurement uncertainty, independent scale calibration, and mesh-metric normalization are not yet available.*

Keywords: 3D scanning; active NIR scanner; mini booth; RMSE; mesh analysis.

1. Introduction

Three-dimensional object visualization allows the shape and surface of a product to be observed from many angles, which makes it relevant for promotion, documentation, education, and digital asset development [1], [4]. Earlier studies have largely used close-range photogrammetry and Structure from Motion to build 3D models from overlapping images [2], [5]-[8]. That approach is effective, but its quality depends on the number of images, the amount of overlap, surface texture, lighting, and the accuracy of camera orientation. More recent work has shifted towards active optical acquisition, in which structured light or an infrared pattern is projected onto the surface and the deformation of that pattern is decoded into depth. Reviews of this field converge on a consistent finding: active systems remove the dependence on image matching and photographic texture, but they remain governed by the optical behaviour of the surface itself, and strongly reflective and transparent materials are identified as the dominant unsolved failure mode [16], [17]. The mitigations reported in that literature are largely acquisition-side - multi-exposure and adaptive fringe projection, polarisation filtering, learning-based recovery of saturated regions, or intrusive matting with an opaque coating - and each carries a cost in time, equipment, or reversibility that is rarely acceptable in routine asset production [16], [18]. The accuracy of low-cost handheld devices under such conditions is still reported far less often than that of industrial systems, which is the gap this study addresses empirically.

This study takes a different route, namely active 3D scanning with the Creality CR-Scan Ferret. The device projects a Near-Infrared (NIR) pattern and records the surface response to form a point cloud and a mesh; the manufacturer specification lists a working distance of 150-700 mm, a point distance of 0.16 mm, a speed of up to 30 fps, and a nominal single-device accuracy of 0.1 mm [9], [10]. Those vendor figures are not treated as workflow accuracy, because the final result is still shaped by the mini booth configuration, object characteristics, reconstruction, cleaning, mesh repair, scaling, and the measurement procedure.

Raw scanner data generally still contain environmental noise, turntable geometry, detached fragments, holes, and topological irregularities. Transparent or reflective surfaces can weaken the NIR response, while deep cavities and stacked components create occlusion. The final project report divides 30 objects into Easy, Medium, and Hard categories to represent that variation. However, a visual category does not automatically guarantee a particular error level; the influence of material, shape, orientation, and scaling has to be read together.

TABLE I. POSITIONING OF THIS STUDY AGAINST THE STUDIES SUMMARIZED IN THE FINAL PROJECT REPORT [15].

Study	Acquisition	Object	Evaluation focus
Sujadi [2]	Close-range photogrammetry	Solid objects	3D model; reconstruction focus
Pardamean & Tolle [5]	Photogrammetry	Temple	Visual completeness of the model
Kafiar [6]	DSLR + UAV	Large objects/landscapes	Combination of acquisition angles
Montusiewicz et al. [12]	3D production and optimization	Cultural heritage	Model readiness for a specific use
This study	Active NIR mini booth	30 objects ≤ 50 cm	RMSE of 30 assets + mesh of 6 samples

Compared with earlier studies, the differentiator of this work is not a new sensor technology but the documentation of an active-scanner workflow for small objects, a coverage of 30 assets, and the use of two evaluation layers: dimensional agreement and topological characteristics. This positioning is more defensible than claiming that the mini booth or 3D scanning itself is a novel finding. The contribution of this study sits at the level of workflow engineering rather than the development of a new scanning algorithm: (1) a mini booth and diffuse-light configuration for acquiring 30 objects with a maximum dimension of 50 cm; (2) a Creality Scan-Blender pipeline for cleaning, remesh/retopology, repairing, and texture baking; (3) dimensional evaluation through RMSE on all assets; and (4) topological characterization through the 3D Print Toolbox on six representative samples. This article also adds descriptive statistical analysis, category comparison, and per-dimension error derived from the same data so that the discussion is more transparent.

2. Methods

A. Design and Test Objects

The study uses a reconstruction-evaluation design applied to 30 physical objects. Each object was placed at the centre of the mini booth, scanned with the CR-Scan Ferret, processed into a textured 3D asset, and then compared with reference physical measurements. The final project report [15] groups the objects into ten Easy, ten Medium, and ten Hard items. Easy is dominated by matte surfaces and visual features that are easy to track; Medium has smoother, slightly reflective, or hollow shapes; Hard covers reflective, transparent, or dark surfaces and complex geometry. That classification is an internal operational category, not a universal scanning-quality standard.

TABLE II. OBJECT CLASSIFICATION SUMMARIZED FROM THE FINAL PROJECT REPORT [15].

Category	n	Operational characteristics	Examples
Easy	10	Matte/textured; relatively simple shape	Perfume bottle, Nailong toy, whiteboard eraser, air-freshener bottle
Medium	10	Slightly reflective/smooth or hollow	Drinking bottle, air-freshener box, teapot, controller
Hard	10	Reflective/transparent/dark or complex geometry	Gundam, diecast, glass bottle, action figure

B. Devices and Configuration

The main device is the NIR-based Creality CR-Scan Ferret. Acquisition data were processed on a laptop with an Intel Core i5-12450HX processor, 12 GB DDR5 RAM, and an NVIDIA GeForce RTX 3050 6 GB. The reported software comprises Creality Scan v3.340, Blender v4.3.2, Python 3.10, and the Open3D library for reading meshes and extracting dimensions. The manufacturer specification and the computing configuration are used to document the experimental environment, not as evidence of final performance. The mini booth uses diffuse light to reduce hard shadows and to keep colour and texture legible. The final project report does not yet report illuminance values, colour temperature, measured lamp positions, the exact scanner-to-object distance for every asset, turntable speed, or the effective number of frames. Those gaps are recorded as limits on reproducibility and are not filled with assumptions.

TABLE III. DEVICES AND PROCESSING ENVIRONMENT.

Component	Reported specification	Function
CR-Scan Ferret	NIR; 150-700 mm; up to 30 fps	Point cloud/mesh acquisition
Mini booth	Objects ≤ 50 cm; diffuse light	Placement and lighting
Laptop	i5-12450HX; 12 GB RAM; RTX 3050 6 GB	Processing
Software	Creality Scan 3.340; Blender 4.3.2; Python/Open3D	Reconstruction, optimization, evaluation

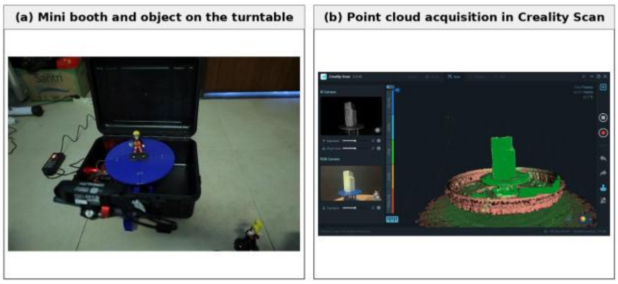

Figure 1. Capture of the acquisition configuration: (a) mini booth and object on the turntable; (b) point cloud in Creality Scan. Source: Final project report [15].

That scheme is a procedural representation. The final project report does not report booth dimensions, lamp positions in coordinates, or the actual distance per object. The 150-700 mm figure in the image is therefore the nominal working range of the device, not a verified distance for every test.

C. Asset Production Pipeline

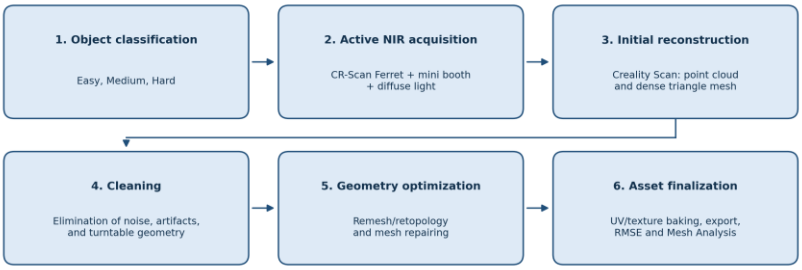

Figure 2. Production and evaluation pipeline summarized from the final project report [15].

Acquisition produces point cloud data and a dense triangle mesh. The initial files were moved into Blender to remove noise, artifacts, and turntable geometry. The remesh/retopology stage tidies the polygon distribution, mesh repairing closes or fixes open areas, and texture baking projects RGB camera colour data onto the model UV. The final model is exported as a 3D asset together with its texture. The report shows a comparison of raw scan and reconstruction results, including the texture baking process on the Air-Freshener Bottle, Perfume Bottle, Air-Freshener Box, Teapot, Custom Gundam, and Mobile Armor Hashmal. The use of Blender and 3D model optimization is supported by [11]-[13].

D. Visual Evidence of Data Transformation

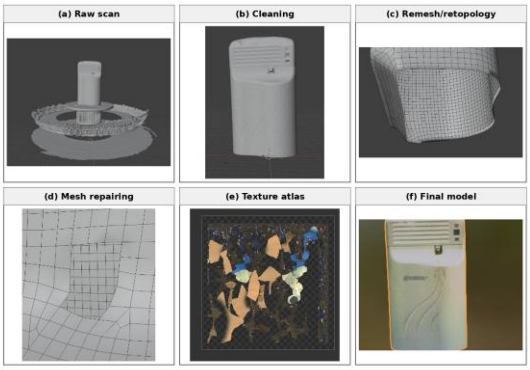

Figure 3. Capture of the data transformation from raw scan to final model: (a) raw scan and turntable; (b) cleaning; (c) remesh/retopology; (d) mesh repairing; (e) texture atlas; and (f) final model. Source: Final project report [15].

The captures in Figure 3 show that the scanner output does not immediately become the final asset. At the raw scan stage, the object geometry is still mixed with the turntable, the floor, and environmental fragments. Cleaning separates the main object, while remesh/retopology rearranges the face distribution so that the model is easier to edit. This stage changes the vertex and face structure, so the original texture information cannot always be preserved directly. Mesh repairing is used on holed or disconnected areas, after which texture baking projects the RGB colour information back onto the UV map of the optimized mesh. The final textured form is therefore a cumulative result of acquisition and post-production, not of the sensor alone. The report does not state the face count before and after retopology, so these captures are used as evidence of process traceability and are not used to claim a polygon reduction ratio or a quantitative rendering improvement.

E. Dimensional Evaluation and Additional Analysis

Physical measurement covers width (X), length/depth (Y), and height (Z). Reference dimensions were taken with manual instruments: a vernier calliper for spans up to approximately 15 cm and a steel measuring tape for larger objects [15]. Each dimension was recorded once per object by a single operator. The source report does not document the brand, nominal resolution, calibration status, or verified repeatability of either instrument, and that omission is stated here rather than reconstructed after the fact. Its consequence can nevertheless be bounded: the reading resolution of instruments of this class is of the order of 0.05 mm for a calliper and 1 mm for a tape, which is one to two orders of magnitude smaller than the RMSE values reported below (0.02-6.18 cm). Instrument resolution is therefore not a plausible driver of the observed error. What cannot be bounded is the operator-dependent component, particularly the definition of the measurement edge on irregular, curved, or armoured silhouettes, because no repeated readings exist from which to estimate it. Digital dimensions were extracted from the maximum mesh extents using a Python/Open3D script. For the i-th asset, RMSE is computed as in (1), and the headline value of the article is the mean of the 30 per-asset RMSE values, not a single RMSE formed from all pooled coordinates.

$$\mathrm{RMSE}_i = \sqrt{\frac{(X_{3\mathrm{D}}-X_{\mathrm{ref}})^2+(Y_{3\mathrm{D}}-Y_{\mathrm{ref}})^2+(Z_{3\mathrm{D}}-Z_{\mathrm{ref}})^2}{3}} \quad (1)$$

The internal thresholds of the final project report [15] are Very Good (< 1 cm), Good (1-< 3 cm), Fair (3-< 5 cm), and Poor (≥ 5 cm). This article adds mean, SD, median, IQR, 95% confidence interval, signed bias (3D model minus physical), MAE per dimension, and an exploratory Kruskal-Wallis test to compare the three categories. The test describes the pattern in the available data and does not prove a causal relationship between material or geometry and error.

Scale determination. The scale of every reconstructed model derives solely from the internal metric calibration of the scanner. The CR-Scan Ferret outputs geometry already expressed in millimetres, and no model was rescaled, normalized, or fitted to any physically measured dimension at any stage of cleaning, retopology, mesh repair, or export. No physical scale bar or calibrated reference artefact was placed in the mini booth [15]. The physical dimensions therefore enter the analysis only as the reference term of (1); they are never an input to the reconstruction. The validation is consequently not circular, because no object dimension is used both to set the scale and to test it. The cost of that independence is that the workflow inherits the calibration error of the sensor with no means of detecting or correcting it, which is the most likely origin of the systematic positive bias reported in Section III-E. Placing a calibrated scale bar or a certified gauge block of known length inside the booth, and reporting the measured-versus-nominal length of that reference alongside each scan, is recommended for subsequent work; it would supply the independent scale check that the present dataset lacks.

Bounding-box convention. Digital dimensions were extracted automatically from the cleaned. plymeshes by a Python script (cek_dimensi.py) built on the open-source evaluate_3d_reconstruction_lib and Open3D, which returns the maximum spatial extent of the vertex set along the global X, Y, and Z axes [15]. This is an axis-aligned bounding box (AABB), and it is therefore sensitive to the orientation in which each mesh happens to sit in the global frame: a model tilted relative to the axes yields an AABB that is never smaller, and usually larger, than the true extent of the object. An oriented bounding box (OBB), computed from the principal axes of the vertex distribution, removes that dependence and is the more defensible convention for dimensional validation. The present figures could not be recomputed under an OBB because this article reuses the tabulated results of the source report rather than the mesh files themselves. Re-running both conventions on the same meshes and reporting the per-object AABB-OBB difference is therefore a priority for the follow-up study, since it would separate genuine reconstruction error from orientation-induced inflation - a distinction made directly relevant by the positive length and width bias in Table VIII.

Repeatability. Each object was scanned once and measured once. The dataset contains no within-object replication, and no repeatability, reproducibility, or measurement-uncertainty statistic can be derived from it. The RMSE values below describe the agreement achieved on a single realization of the workflow per object; they are not an estimate of the precision the workflow would attain on repetition. A replication design of at least three independent scans and three independent physical measurements on representative Easy, Medium, and Hard objects, reported as within-object standard deviation and coefficient of variation, is required before any precision claim can be made, and is planned as the immediate extension of this work.

F. Mesh Analysis

Topology was inspected using the Blender 3D Print Toolbox [14]. The recorded parameters are Non-manifold Edges, Bad Contiguous Edges, Intersect Faces, Shells, Zero Faces/Edges, Thin Faces, Non-flat Faces, Sharp Edges, and Overhang Faces. In line with the scope of the final project report, Mesh Analysis was applied to six samples selected by stratified purposive sampling: two Easy (Air-Freshener Bottle, Perfume Bottle), two Medium (Air-Freshener Box, Teapot), and two Hard (Custom Gundam, Mobile Armor Hashmal). Within each stratum the pair was chosen to span the topological extremes observed during post-production rather than to represent the stratum on average: one object with a closed, convex, single-shell body, and one with cavities, thin walls, or stacked and overlapping components. The six therefore bracket the range of mesh behaviour the workflow produces, from the simplest closed surface to the most fragmented, and they deliberately include the two objects whose reconstruction was most difficult. They are not a random sample and are not statistically representative of the 30 assets; conclusions drawn from them describe the span of possible outcomes, not their frequency across the full set. The available values are raw counts and have not been normalized against the number of faces/edges of each model; the Overhang parameter is mainly relevant to 3D printing orientation and does not directly indicate a visual defect in digital use.

TABLE IV. LIMITED MEANING OF THE MESH ANALYSIS PARAMETERS.

Parameter	Interpretive meaning
Non-manifold Edges	Boundaries or topological junctions that do not have a manifold configuration
Shells	Number of connected geometry components; Shells = 1 is not automatic proof of watertightness
Intersect Faces	Mutually penetrating faces; may trigger repair/printing problems
Zero/Thin/Non-flat	Degenerate or problematic faces at the inspection tolerance
Overhang Faces	Sensitive to orientation and more relevant to 3D printing

3. Results and Discussion

A. Production Results and RMSE Distribution

The workflow produced 30 textured 3D assets. Per-asset RMSE ranges from 0.02 to 6.18 cm with a mean of 2.00 cm, SD of 1.61 cm, median of 1.80 cm, and an IQR of 0.61-2.83 cm. The 95% confidence interval of the mean is 1.40-2.60 cm. The wide spread shows that a single mean value is not enough to describe the variation in performance between objects. The consistency of the formula can be seen in the Custom Gundam. The physical and model widths are 11.00 and 12.33 cm; the lengths are 6.50 and 6.78 cm; and the heights are 20.00 and 15.91 cm. The sum of squared differences is 18.5754 cm², so MSE = 6.1918 cm² and RMSE = $\sqrt{6.1918}$ = 2.49 cm. This example confirms that a single RMSE value represents three dimensions of one asset.

TABLE V. EXAMPLE RMSE COMPUTATION FOR THE CUSTOM GUNDAM (2.49 CM).

Dimension	Physical	3D model	Error	Error²
Width (X)	11.00	12.33	+1.33	1.7689
Length (Y)	6.50	6.78	+0.28	0.0784
Height (Z)	20.00	15.91	-4.09	16.7281

Based on the internal thresholds, 12 assets (40%) are Very Good, 11 assets (36.7%) Good, 5 assets (16.7%) Fair, and 2 assets (6.7%) Poor. Thus 23 of the 30 assets fall below 3 cm. These categories are an operational interpretation of the study; they must not be treated as a universal standard for every application. Tolerances for web visualization, AR/VR, dimensional inspection, and 3D printing can differ.

TABLE VI. INDIVIDUAL RMSE OF THE 30 ASSETS; SORTED FROM THE LOWEST ERROR.

Asset	Category	RMSE (cm)	Internal criterion	Asset	Category	RMSE (cm)	Internal criterion
Woven Basket	Medium	0.02	Very Good	Dragon Fruit	Easy	1.88	Good
Perfume Bottle	Easy	0.23	Very Good	Gundam Schwarzette	Hard	1.97	Good
Air-Freshener Bottle	Easy	0.41	Very Good	Teapot	Medium	2.20	Good
Wireless Mouse	Medium	0.41	Very Good	Custom Gundam	Hard	2.49	Good
Plain Glass	Medium	0.44	Very Good	Flower Vase	Medium	2.54	Good
VR Controller	Easy	0.50	Very Good	Bar Soap	Easy	2.67	Good
Asuma Sirotobi	Hard	0.58	Very Good	Gundam Hashmal	Hard	2.77	Good
Air-Freshener Box	Medium	0.59	Very Good	Gundam GM Spartan	Hard	2.85	Good
Whiteboard Eraser	Easy	0.65	Very Good	AF Naruto	Hard	3.01	Fair
Drinking Bottle	Medium	0.70	Very Good	Fabric Pencil Case	Easy	3.60	Fair
Nailong Toy	Easy	0.74	Very Good	AF Ultraman	Medium	3.62	Fair
Keychain	Easy	0.79	Very Good	Alphard Diecast Car	Hard	4.16	Fair
Leather Wallet	Medium	1.11	Good	AF Kamen Rider	Hard	4.43	Fair

Asset	Category	RMSE (cm)	Internal criterion	Asset	Category	RMSE (cm)	Internal criterion
Game Controller	Medium	1.47	Good	Glass Bottle	Hard	5.13	Poor
Creality Box Cover	Easy	1.72	Good	AF Astray Gold	Hard	6.18	Poor

B. Relationship Between Difficulty Category and Error

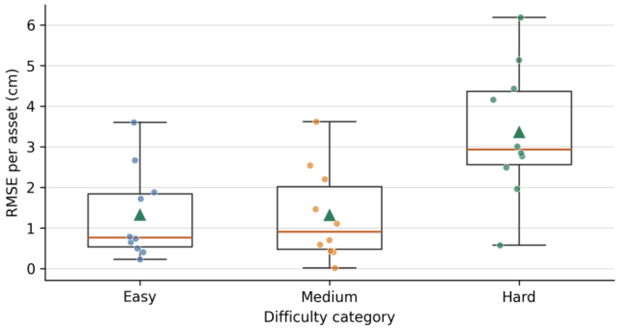

Figure 4. RMSE distribution by difficulty category.

TABLE VII. SUMMARY OF RMSE BY CATEGORY.

Category	n	Mean	Median	Min-max (cm)
Easy	10	1.32	0.77	0.23-3.60
Medium	10	1.31	0.91	0.02-3.62
Hard	10	3.36	2.93	0.58-6.18

Easy and Medium objects have almost the same mean, 1.32 and 1.31 cm respectively. This similarity shows that the category label is not determined by a single factor. Several Medium objects, such as the Woven Basket (0.02 cm), the Wireless Mouse (0.41 cm), and the Plain Glass (0.44 cm), still produce high agreement. Conversely, several Easy objects, such as the Fabric Pencil Case (3.60 cm), the Bar Soap (2.67 cm), and the Dragon Fruit (1.88 cm), show larger errors. A shape that is easy to see is not necessarily easy to scale or align.

The Hard category has a mean of 3.36 cm and a median of 2.93 cm. The Kruskal-Wallis test yields $H = 9.76$ and $p = 0.0076$, so there is a difference in distribution between categories in this data set. However, the result does not isolate the variables of material, reflectance, size, geometry, and orientation. Asuma Sirotobi, which belongs to the Hard group, in fact obtained an RMSE of 0.58 cm; the difficulty category is therefore a tendency, not a deterministic predictor. Nonparametric pairwise analysis shows that Easy and Medium do not differ (Mann-Whitney $p = 0.970$), whereas Hard is higher than both Easy and Medium; after Holm correction, both comparisons sit at around $p = 0.022$. These results remain exploratory because each group contains only ten samples and the categories are formed from a combination of several physical characteristics.

C. Visual Evidence of Representative Reconstruction Results

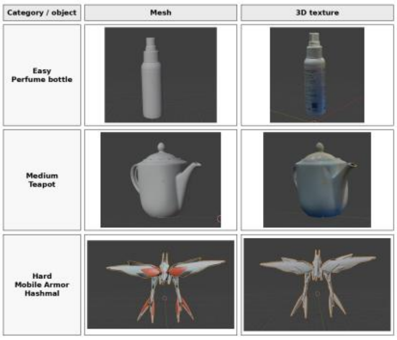

Figure 5. Capture of representative reconstruction results for the Easy, Medium, and Hard categories. Source: Final project report [15].

The Perfume Bottle (Easy) retains its cylindrical contour and label detail after texture baking, at an RMSE of 0.23 cm. The Teapot (Medium) remains recognizable in body and texture, but its handle, spout, lid, and concave areas invite occlusion: RMSE 2.20 cm, with 542 non-manifold edges despite a single shell. Mobile Armor Hashmal (Hard) still presents a legible silhouette of wings and main components at an RMSE of 2.77 cm, yet its internal cavities, stacked parts, and thin components carry 14,945 non-manifold edges across seven shells. Visual legibility, dimensional agreement, and topological integrity are therefore three distinct attributes; a recognizable model is not necessarily closed or printable. This is descriptive visual evidence only. No independent assessors, texture sharpness metrics, colour difference, or shape completeness scores were used, so terms such as “sharp” or “realistic” are avoided as claims.

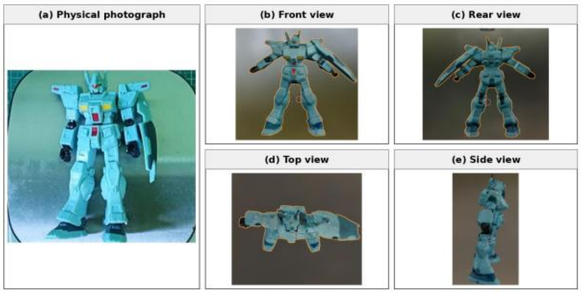

Figure 6. Capture of the traceability of the Custom Gundam from physical photograph to multi-angle 3D result. Source: Final project report [15].

The Custom Gundam matters because its single RMSE of 2.49 cm conceals a non-uniform error pattern: width is 1.33 cm and length 0.28 cm larger than physical, while height is 4.09 cm smaller. The aggregate value states the magnitude of the combined error but hides its direction and dominant dimension, which is why signed error per axis must be reported before any rescaling decision. The multi-angle views in Figure 6 confirm a silhouette that remains recognizable from several directions, but this must be read alongside the topology: three shells and 5,318 intersect faces. With no repeated scan isolating orientation, scaling, and occlusion, these remain candidate causes rather than established ones.

D. Analysis of Low- and High-Error Cases

The lowest errors belong to texture-rich objects that can be captured from many directions: Woven Basket 0.02 cm, Perfume Bottle 0.23 cm, Air-Freshener Bottle 0.41 cm, Air-Freshener Box 0.59 cm, and Drinking Bottle 0.70 cm. Error rises for hollow and complex shapes - Teapot 2.20 cm, Custom Gundam 2.49 cm, Mobile Armor Hashmal 2.77 cm, GM Spartan 2.85 cm, Naruto 3.01 cm - where concave parts, wings, shields, small joints, and mutually occluding areas reduce coverage and increase the need for repair. The two highest errors are the Glass Bottle at 5.13 cm and AF Astray Gold at 6.18 cm, both consistent with the reduced NIR response expected from transparent and reflective surfaces and with the scale drift the source report acknowledges. In none of these bands, however, do the data separate occlusion from scaling or bounding-box orientation: each object was scanned once, and no object was tested before and after matte spray or against a scale bar. These readings are therefore process interpretations, not causal proof that any single factor dominates.

E. Signed Error per Dimension and Scale Drift

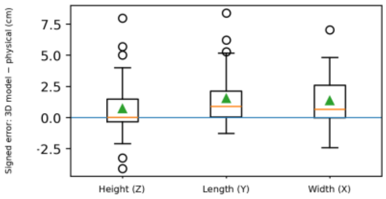

Figure 7. Signed error of the 3D models against the physical measurements.

TABLE VIII. DIMENSIONAL ERROR; BIAS = 3D MODEL − PHYSICAL SIZE.

Dimension	Bias	MAE	SD of error	Error range (cm)
Height	+0.71	1.61	2.46	-4.09 to +7.97
Length	+1.52	1.75	2.25	-1.30 to +8.39
Width	+1.35	1.60	2.04	-2.42 to +7.05

On average the 3D models are 0.71 cm larger in height, 1.52 cm larger in length, and 1.35 cm larger in width. The MAE of the three dimensions lies between 1.60 and 1.75 cm. The positive bias in length and width is consistent with a tendency toward scale enlargement, but the error spread remains wide and several objects were reduced instead. This finding strengthens the recommendation to add a scale bar or an independent control distance on the turntable.

Besides scale drift, an axis-aligned bounding box can grow if the model is tilted relative to the X-Y-Z axes. Future work should document orientation, apply registration to a reference coordinate frame, compare axis-aligned and oriented bounding boxes, and store the scaling transformation. A dimension used for scaling must not be reused as an independent evaluation measure without explanation.

F. Error Normalized to Object Size

Because the physical sizes of the objects differ, absolute RMSE was also examined secondarily against the physical bounding-box diagonal. For the i-th asset, the diagonal is given by (2) and the normalized error by (3). This normalization does not replace RMSE in centimetres, but it helps compare the magnitude of the error against the scale of the object.

$$d_i = \sqrt{{H_i}^2 + {L_i}^2 + {W_i}^2} \tag{2}$$

$$\mathrm{NRMSE}_{\mathrm{diag},i} = \frac{\mathrm{RMSE}_i}{d_i} \times 100\% \tag{3}$$

TABLE IX. NRMSE STATISTICS AGAINST THE BOUNDING-BOX DIAGONAL AND THE SIZE-RMSE RELATIONSHIP.

Statistic	Value
Mean NRMSE_diag	11.80%
Median	7.61%
IQR	3.60-13.73%
Range	0.10-66.16%
Pearson: diagonal vs RMSE	r = 0.040; p = 0.832
Spearman: diagonal vs RMSE	ρ = 0.089; p = 0.638

The largest relative values occur for AF Astray Gold (66.16%), AF Kamen Rider (39.39%), the Glass Bottle (24.17%), the Alphard Diecast Car (23.98%), and the Ultraman action figure (22.02%). Neither the Pearson nor the Spearman correlation shows a meaningful relationship between physical diagonal and RMSE across the 30 samples. This means that object size alone does not explain the variation in error; material, geometry, orientation, occlusion, and scaling still have to be examined together. This analysis is a recomputation of the same data, not a new experiment.

G. Mesh Analysis of Six Samples

TABLE X. MESH ANALYSIS RAW COUNTS FOR THE SIX REPRESENTATIVE SAMPLES [15].

Sample	Non-manifold	Shells	Intersect	Zero faces	Zero edges	Thin faces	Non-flat	Overhang
Air-Freshener Bottle	0	1	53	661	0	254	38	6,058
Perfume Bottle	0	1	6	2,734	85	37	57	133
Air-Freshener Box	10	24	38	8	0	9	0	1,107
Teapot	542	1	2	272	24	11	26	19,826
Custom Gundam	0	3	5,318	13,441	337	6,876	108,786	60,701
Hashmal	14,945	7	26	4,158	171	27	151	37,535

The Air-Freshener Bottle and the Perfume Bottle have Non-manifold Edges = 0 and Shells = 1. This combination supports a single closed topology at the inspection tolerance used, but it does not automatically remove the Intersect Faces, Zero Faces, Thin Faces, or other artifacts that were found. The term watertight should therefore only be used after all criteria have been defined and verified, not on the basis of a single parameter.

The Air-Freshener Box has 24 shells, indicating many separate components even though Non-manifold Edges is only 10. The Teapot has one shell but 542 non-manifold edges; object connectivity is therefore not identical to topological closure. The Custom Gundam has Non-manifold Edges = 0 but three shells and 5,318 intersect faces, so a watertight label in the earlier table is not defensible without cleanup and re-inspection.

Hashmal is the heaviest case, with 14,945 non-manifold edges and seven shells. This result is consistent with wings, internal cavities, and stacked components that produce many uncaptured or detached areas. For digital visualization the model may still be acceptable if the silhouette, texture, 360° rotation, and absence of visual artifacts satisfy an acceptance checklist. For 3D printing, non-manifold edges and multiple shells must be repaired first.

Comparison of mesh figures across models must remain cautious, because Table X reports raw defect counts while the total face and edge count of each asset is not recorded in the source report [15]. A model with millions of faces will accumulate a higher raw count at the same defect density, so the raw figures rank mesh size as much as mesh quality. The 14,945 non-manifold edges of Hashmal and the 108,786 non-flat faces of the Custom Gundam cannot be read as evidence that those meshes are proportionally worse than the Perfume Bottle until both are expressed per unit of mesh size. The appropriate normalization is a defect rate: defects per 10,000 faces for face-based parameters (Intersect, Zero, Thin, Non-flat, Overhang) and defects per 10,000 edges for edge-based parameters (Non-manifold, Bad Contiguous, Sharp), with Shells left as an absolute count because it measures connectivity rather than defect density. Expressed that way the six samples become directly comparable to one another and portable to other studies. These rates could not be computed retrospectively for this article, because the face and edge totals were not captured at inspection time and the source meshes were not re-opened; the values are therefore presented as raw counts with that limitation stated, rather than estimated from assumed mesh sizes. Re-inspecting the six meshes to log face and edge totals and republishing Table X as defect rates is the first correction planned for the extended dataset, together with a fixed and reported inspection tolerance so that the Zero, Thin, and Non-flat counts become reproducible across operators. Overhang Faces are also separated from visual quality because that parameter is affected by the orientation of the object relative to the printing direction.

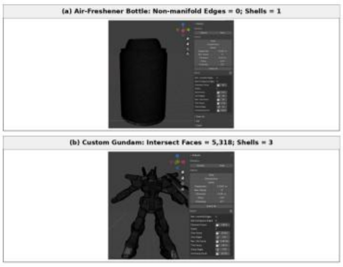

Figure 8. Capture of the 3D Print Toolbox: (a) Air-Freshener Bottle; (b) Custom Gundam. Source: Final project report [15].

The Air-Freshener Bottle capture shows Non-manifold Edges = 0 and Shells = 1, but 53 intersect faces, 661 zero faces, and 254 thin faces remain. In the Custom Gundam, Non-manifold Edges is also 0, yet the object consists of three shells and has 5,318 intersect faces and 13,441 zero faces. This evidence reinforces that a single parameter is not enough to declare a mesh watertight; all indicators must be read together with the intended use of the asset.

TABLE XI. INTERPRETATION FRAMEWORK FOR ASSET USE BASED ON THE FINDINGS; A RECOMMENDATION, NOT A NEW TEST RESULT.

Purpose	Minimum inspection	Interpretation
Web/AR/VR	360° silhouette, main texture, no large holes	Usable with documented defects
Further editing	Shells, non-manifold, intersect/degenerate faces, UV	Cleanup required before rigging/animation
3D printing	Boundary, self-intersection, shell, thickness, overhang	Not yet demonstrated; specific repair and validation required

For web, AR, or VR visualization, small defects can be tolerated as long as they do not disturb the silhouette and the 360° rotation. For rigging, animation, or fabrication, the requirements must be stricter. This study has not performed rigging or 3D printing validation, so the related rows are used as interpretation limits and as an agenda for further inspection.

H. Synthesis of Process, Limitations, and Improvements

Compared with the photogrammetry pipeline of earlier studies, an active scanner reduces the dependence on matching hundreds of photographs, but it does not remove the limitations of surface behaviour and occlusion. The data show that trade-off: regular objects can be reconstructed with a low RMSE, whereas glass, metallic surfaces, cavities, and stacked components still require special treatment and post-production. Active scanning and photogrammetry should therefore be seen as complementary approaches rather than as a superior-inferior pair, in the absence of a comparative experiment.

That trade-off is consistent with the published literature rather than particular to this booth. Reviews of structured-light measurement on highly reflective surfaces report the same failure signature - saturated or missing returns over specular regions, propagating into geometry that is either absent or displaced - and treat it as an intrinsic limit of the triangulation principle rather than an implementation defect [16]. The transparent-object literature reaches a stronger conclusion still, holding that conventional projected-pattern systems cannot recover a transparent surface without either an intrusive opaque coating or a fundamentally different optical model such as refraction-based or tomographic reconstruction [17], [18]. Read against that background, the two worst cases in this dataset are unsurprising: the Glass Bottle at 5.13 cm and AF Astray Gold at 6.18 cm fail in precisely the manner those studies predict, and their errors are better attributed to acquisition physics shared by every NIR and structured-light device in this class than to the mini booth configuration. The practical implication also matches the literature: within this workflow's cost envelope, matte coating is the only viable mitigation, so objects that cannot be coated should be routed out of the active-scanning pipeline at the preparation stage rather than scanned and repaired afterwards. Direct numerical comparison with those studies nevertheless remains inappropriate, because they report accuracy against calibrated artefacts under laboratory conditions in millimetres or micrometres, whereas the present figures are centimetre-scale agreement against manual reference measurements on uncalibrated consumer objects.

Overall, the pipeline produced all 30 assets and most RMSE values fall below 3 cm. The strength of the study lies in the diversity of objects covered and in the traceability of the process from scan to evaluation. Its constraints are those set out in Section II-E - single-scan acquisition, sensor-derived scale, AABB extraction, and undocumented instrument uncertainty - to which should be added the absence of per-object distance and lighting logs, polygon counts, and a formal 360° acceptance checklist. The category statistics, signed error, and NRMSE figures are moreover a secondary analysis of the 30 data rows already tabulated in the source report [15] rather than the product of new scanning, and the Easy, Medium, and Hard strata confound shape, colour, reflectivity, transparency, texture, and occlusion, none of which was manipulated in a controlled way. The between-category RMSE difference therefore cannot be read causally, and the results support the feasibility of the workflow for producing initial visual assets, not a claim of metrological precision, watertightness, or manufacturing readiness.

I. Operational Implications for Asset Production

Cross-case findings can be translated into a production decision protocol that separates acquisition success, post-production success, and fitness for use. This separation matters because an object may look good after texture baking yet still carry a dimensional error or a topological defect. Conversely, a low RMSE value does not guarantee a complete texture and a mesh that is ready for rigging or printing.

TABLE XII. PROPOSED DOCUMENTATION AND PRODUCTION DECISION PROTOCOL DERIVED FROM THE FINDINGS.

Stage	Recorded data	Decision and action
Preparation	Material, reflectivity, cavities, physical dimensions, scale bar	Use matte spray/markers or change orientation for at-risk objects
Acquisition	Working distance, coverage, tracking, lighting, number of passes	Repeat from another angle if tracking is lost or an area is occluded
Post-production	Raw/clean mesh, face count, repair log, UV and texture baking	Repair shells/intersections; store versions and the scaling transformation
Validation	RMSE, signed error, NRMSE, mesh rate, 360° visual checklist	Accept according to purpose; re-scan or restrict use on failure

At the preparation stage, transparent or highly reflective objects must be treated as high risk rather than run with the same parameters as matte objects, and a control distance or scale bar must be recorded independently of the three dimensions used for evaluation. Concave areas, undersides, and stacked components need additional passes or a change of orientation to reduce blind spots. In post-production, the raw scan, clean mesh, remesh, repair, and texture-baking versions should be stored separately so that changes can be audited. The final decision must state the context of use: interactive visualization tolerates minor invisible defects, whereas rigging and 3D printing demand stricter topology. Table XII is a recommendation derived from the findings, not a prospectively tested acceptance threshold.

4. Conclusions

This study documents a workflow for producing 30 small-scale 3D assets using the CR-Scan Ferret, a mini booth, diffuse light, Creality Scan, Blender, Python, and Open3D. Mean per-asset RMSE is 2.00 cm (SD 1.61 cm; range 0.02-6.18 cm), and 23 assets fall within the Very Good or Good band. Hard objects show higher error than Easy and Medium in the exploratory analysis, but the difficulty category does not determine the outcome absolutely. Errors carry a positive bias in length and width, so scaling and bounding-box orientation require calibration. Mesh Analysis on six samples varies widely: two regular bottles reach Non-manifold Edges = 0 with a single shell, whereas complex objects show multiple shells, intersect faces, and high non-manifold counts. The results do not support a claim that all assets are watertight.

The workflow is usable as an initial pipeline for digital visualization after per-object inspection and repair. Further development needs to add a scale bar, a matte-spray protocol for reflective surfaces, lighting and distance measurement, repeated scans, measuring-instrument validation, oriented bounding boxes, normalization of mesh metrics, and separate acceptance checklists for visualization and for 3D printing.

Acknowledgements

The authors thank the D3 Multimedia Broadcasting Technology Study Program, Department of Creative Multimedia Technology, Politeknik Elektronika Negeri Surabaya, for the laboratory facilities and the scanning equipment used in this study. The dimensional data, individual RMSE results, process documentation, and six Mesh Analysis results for the 30 assets are held in the final project report [15]; no public repository has yet been declared for the 3D models, raw images, or Python scripts.

References

[1] M. Janiszewski et al., “Rapid photogrammetry with a 360-degree camera for tunnel mapping,” Remote Sensing, vol. 14, no. 21, art. 5494, 2022. DOI: https://doi.org/10.3390/rs14215494
[2] D. Sujadi, “3D Modelling Obyek Kerapatan Tinggi Menggunakan Metode Fotogrametri Jarak Dekat,” Tugas Akhir, Institut Teknologi Nasional Malang, Malang, Indonesia, 2018.
[3] M. Tjahjadi and T. Djauhari, “Modeling 3 Dimensi Sungai dari Foto Udara,” Institut Teknologi Nasional Malang, pp. 1-9, 2017.
[4] E. Ardhianto, W. Hadikurniawati, and E. Winarno, “Augmented reality objek 3 dimensi dengan perangkat ARToolkit dan Blender,” Dinamik, vol. 17, no. 2, pp. 107-117, 2012.
[5] B. S. Pardamean and H. Tolle, “Pembuatan Objek 3D Candi Badut Menggunakan Metode Photogrammetry,” Jurnal Pengembangan Teknologi Informasi dan Ilmu Komputer, vol. 5, no. 6, pp. 2408-2417, 2021.
[6] M. T. Kafiar, “Visualisasi 3D Modelling dari Hasil Kombinasi Kamera DSLR dan UAV dengan Metode Close Range Photogrammetry,” Tugas Akhir, Institut Teknologi Nasional Malang, Malang, Indonesia, 2020.
[7] T. Luhmann, S. Robson, S. Kyle, and J. Boehm, Close-Range Photogrammetry and 3D Imaging, 4th ed. Berlin, Germany: De Gruyter, 2023.
[8] M. J. Westoby, J. Brasington, N. F. Glasser, M. J. Hambrey, and J. M. Reynolds, “Structure-from-Motion Photogrammetry: A low-cost, effective tool for geoscience applications,” Geomorphology, vol. 179, pp. 300-314, 2012. DOI: https://doi.org/10.1016/j.geomorph.2012.08.021
[9] Creality, “CR-Scan Ferret Product Page,” 2023. [Online]. Available: https://www.creality.com/products/cr-scan-ferret
[10] Creality 3D, CR-Scan Ferret User Manual and Technical Specifications. Shenzhen, China: Creality 3D Technology, 2023.
[11] Z. Taeonisokhi, N. Berto, and B. S. Soni, “Pengenalan Dasar Aplikasi Blender 3D dalam Pembuatan Animasi 3D,” Jurnal ABDIMAS Budi Darma, vol. 1, no. 1, pp. 1-6, 2020.
[12] J. Montusiewicz, M. Barszcz, and S. Korga, “Preparation of 3D models of cultural heritage objects to be recognised by touch by the blind: Case studies,” Applied Sciences, vol. 12, no. 23, art. 11910, 2022. DOI: https://doi.org/10.3390/app122311910
[13] Blender Foundation, “Blender - a 3D creation suite,” 2024. [Online]. Available: https://www.blender.org
[14] Blender Foundation, “3D Print Toolbox,” Blender Manual, 2023. [Online]. Available: https://docs.blender.org
[15] P. U. Handayu, “Produksi Aset 3D 360° pada Mini Booth Menggunakan Kamera 3D,” Proyek Akhir, Politeknik Elektronika Negeri Surabaya, Surabaya, Indonesia, 2026.
[16] X. Zhao, T. Yu, D. Liang et al., “A review on 3D measurement of highly reflective objects using structured light projection,” The International Journal of Advanced Manufacturing Technology, vol. 132, pp. 4205-4222, 2024, doi: 10.1007/s00170-024-13566-z.
[17] “Non-destructive optical measurement of transparent objects: a review,” Light: Advanced Manufacturing, 2025, doi: 10.37188/lam.2025.022.
[18] K. Sharma, M. Rahaman, S. Kumar et al., “Use of structured light in 3D reconstruction of transparent objects,” Applied Optics, vol. 61, no. 5, pp. B314-B321, 2022, doi: 10.1364/AO.444450.